Rheol Acta (2001) 40: 74–85
© Springer-Verlag 2001

ORIGINAL CONTRIBUTION

C. Clasen
W.-M. Kulicke

A convenient way of interpreting steady shear rheo-optical data of semi-dilute polymer solutions

Received: 8 May 2000
Accepted: 12 September 2000

C. Clasen · W.-M. Kulicke (✉)
Institut für Technische
und Makromolekulare Chemie
Universität Hamburg
Bundesstr. 45, 21046 Hamburg
Germany
e-mail: Kulicke@chemie.uni-hamburg.de

Abstract Rheo-mechanical and rheo-optical investigations were carried out with the aim of determining the influence of deformation and orientation or disentangling of polymer coils on the flow behavior in the non-Newtonian region of the flow curve, for a moderately concentrated network solution. To avoid the influence of polydispersity this was done on a series of narrowly distributed polystyrene standards (dissolved in toluene). By using steady state shear flow measurements it was possible to detect qualitatively a reduction in the entanglement density within the non-Newtonian flow region. Birefringence experiments were able to show that deformation of the polymer coils also occurs in the Newtonian flow region, which has no effect on the flow behavior in this range, whereas in the non-Newtonian flow region the increase in deformation is lower than in the Newtonian range. The flow birefringence and its orientation can be described over the whole range of the flow curve with a newly developed equation system (Eq. 8 and 14) derived from the stress states of a sheared solution using the stress-optical rule. Starting from these equations, it could be shown, that in the Newtonian flow region a mastercurve in form of a reduced birefringence $\Delta n'/\eta_0 = f(\dot{\gamma})$ and a reduced orientation $\phi = f(\dot{\gamma}/\dot{\gamma}_{crit})$ can be plotted, independent from concentration and molar mass. A comparison of the experimentally determined orientation angle and birefringence curve form with theoretical deformations and orientations of polymer coils in a solution state, without intermolecular interactions, was able to demonstrate that the flow behavior of a moderately concentrated network solution is determined decisively (approximately to 85%) by the disentanglement.

Key words Polystyrene standards · Rheo-optic · Mastercurve · Orientation · Disentanglement

List of abbreviations and symbols

*	transition from particle solution to network solution
**	transition from moderately concentrated to concentrated
a, b	coefficients of the distribution function
c	concentration
C	stress-optical coefficient
G^A	shear modulus
G_0^A	zero-shear modulus
K	critical overlap parameter
M_w	weight-average molar mass
M_n	number-average molar mass
n	refractive index tensor
$\Delta n'$	flow birefringence
N_1	first normal stress difference
p	pressure, axial ratio

P	associated Legendre polynomial
t	time
T	temperature
ϕ	orientation angle of the birefringence in direction of flow
γ	deformation
$\dot{\gamma}$	shear rate
$\dot{\gamma}_{crit}$	critical shear rate
η	shear viscosity
η_{spec}	specific viscosity
η_0	zero-shear viscosity
$[\eta]$	intrinsic viscosity
κ	displacement factor of the mirror relation
ν_e	number of entanglements
τ	stress tensor
$\Delta\tau$	first main stress difference
τ_I	first main stress
τ_{II}	second main stress
τ_{21}	shear stress
Ψ	orientation in neutral direction
Ψ_1	first normal stress coefficient

Introduction

The reduction in viscosity of polymer solutions and melts above a critical shear rate is of great significance for their processing and application. Various theories have been put forward to date for this non-Newtonian flow behavior. Apart from a reduction in the excluded volume and increasing intramolecular interactions (Peterlin 1960, 1961), together with the influence of a finite extensibility of polymer chains on the flow behavior (Bird et al. 1977), today there are primarily two theories that can be used to explain the flow behavior in various different solution states. Here the description of the solution state is based on the five different solution states suggested by Graessley (Graessley et al. 1967; Graessley 1974) from the entanglement theory, which was extended by Kulicke et al. (Bouldin et al. 1988) for moderately concentrated solutions.

In the case of dilute and moderately concentrated particulate solutions (overlap parameter $c \cdot [\eta] <$ critical overlap parameter $(c \cdot [\eta])^*$), in which intermolecular interactions may be neglected when compared with the intramolecular interactions, hydrodynamic interactions are held responsible for the occurrence of the non-Newtonian flow range (Fixman 1966). In the Newtonian flow range the deformations of the polymer coil caused by shear can be compensated for by the relaxation movement of the polymer segments. If the shear rate exceeds the reciprocal relaxation time of the longest segment, the equilibrium state is disrupted. The increased deformation of the polymer coil and the greater degree of orientation in the shear field that accompanies it mean that there is a decrease in the hydrodynamic radius perpendicular to the direction of shear, and hence a reduction of the viscosity in the non-Newtonian range of shear rates.

Graessley accounted for the structural viscosity of concentrated network solutions ($c > c^{**}$, $c \cdot M_w > (c \cdot M_w)^*$) and melts by means of intermolecular interactions with the aid of the entanglement theory (Graessley 1974). According to this explanation, this solution state contains chain entanglements between interpenetrating polymer coils, which, because of the greater frictional forces, produce a higher viscosity compared with a particulate solution. In the Newtonian flow range the disentanglement caused by the input of shear force is reformed by the relaxation movement of the segments. If the shear rate exceeds the reciprocal relaxation time of the chain segments, then the entanglements can no longer be completely reformed, and the result is a reduction in the entanglement density and hence the viscosity.

Both theories are generally acknowledged in publications (Macosco 1994; Pahl et al. 1995; Elias 1996). However, there is still no explanation as to which cause predominates in the moderately concentrated network solutions ($c \cdot [\eta] > (c \cdot [\eta])^*$; $c < c^{**}$), which constitute an important range for technical applications. In order to answer this question, rheo-mechanical and rheo-optical investigations were carried out on narrowly distributed polystyrene standards in moderately concentrated toluene solution.

Experimental

The samples investigated were commercially available polystyrene standards from Pressure Chemical Co. (Pittsburgh, USA) and Polysciences Inc. (Warrington, USA). The samples were characterized with respect to their molar masses and molar mass distributions ($M_w/M_n = 1.06$–1.30) with the aid of light-scattering experiments (Kniewske and Kulicke 1983). Toluene was added to the samples which were then agitated on a shaker table at room temperature for 8 days until they were fully dissolved.

The rheo-mechanical measurements were performed on rotary rheometers of the types RFS-8500 (Rheometrics Inc., New Jersey, USA) and UDS 200 (Paar Physica, Stuttgart, Germany) with cone-plate geometries.

The apparatus used for rheo-optical investigations was built by ourselves and is described in detail in the references (Johnson et al. 1985; Reinhardt et al. 1995; Kulicke and Ahrendt 1997).

Results and discussion

On account of their narrow molar mass distribution, polystyrene standards in solution and as melts are used as calibration standards and in the past have been the subject of intensive investigations (Grigorescu and Kulicke 2000). The occurrence of pronounced intermo-

lecular interaction with increasing molar mass has already been discovered for melts by Büche. Above a critical molar mass, M_w^*, penetration of the polymer coils occurs and this results in the formation of entanglements of polymers segments of different polymer coils. This leads to a pronounced increase in the zero-shear viscosity, η_0, above the critical molar mass, M_W^*. The zero-shear viscosity, η_0, decreases linearly with the molar mass for molar masses below M_W^* down to ($\eta_0 \sim M_w$), whereas above M_W^* η_0 is proportional to $M_W^{3.4}$ (Bueche 1952).

Similar behavior also occurs in concentrated solutions ($c > c^{**}$) (Baumgärtel and Willenbacher 1996). Here the zero-shear viscosity, η_0, is proportional to the product $c \cdot M_W^{3.4}$ (Fig. 1). It was also possible to confirm this proportionality theoretically on the basis of Graessley's entanglement concept (Graessley 1965, 1967), via the reptation concept according to De Gennes (De Gennes 1971, 1979; DeGennes and Leger 1982) and further observations by Doi (1983) and Doi and Edwards (1978, 1986).

In contrast to this, it was not possible to obtain a master curve in moderately concentrated network solutions ($c \cdot [\eta] > (c \cdot [\eta])^*$; $c < c^{**}$) with the aid of the entanglement or reptation concepts. Admittedly, a pronounced increase in the zero-shear viscosity can also be observed above a critical molar mass and critical concentration. However, the expansion of the polymer coil due to the solvent also has to be taken into account here, the product $c \cdot M_W$ can no longer be applied as a measure for the critical volume ratio (Fig. 2). The influence of the solvent is taken into account if the molar mass is replaced by the intrinsic viscosity $[\eta]$ as a measure for the volume requirement of polymer coils in solution. The zero-shear viscosity, η_0, (or the specific viscosity, η_{spec}) in moderately concentrated solutions ($c < c^{**}$) can then be presented as a function of the overlap parameter $c \cdot [\eta]$ (Kulicke and Kniewske 1984) (Fig. 3). Here the overlap parameter represents a measure of the number of entanglements per unit volume. In this case penetration of the polymer coils occurs above a critical overlap parameter $(c \cdot [\eta])^*$, with the transition range being broader than in concentrated solutions.

For moderately concentrated network solution the viscosity of the Newtonian flow range, η_0, can be described from the master curve in Fig. 3 with the aid of empirical structure-property relationships, according to Kulicke and Kniewske (1984). They permit the zero-shear viscosity, η_0, to be calculated for a given polymer-solvent system (p, T = constant) from the molecular parameters of concentration, c, and molar mass, M_W, taking into account the Kuhn-Mark-Houwink-Sakurada relationship (Flory 1975). The following applies for the polystyrene in toluene system under consideration here (Kulicke and Kniewske 1984):

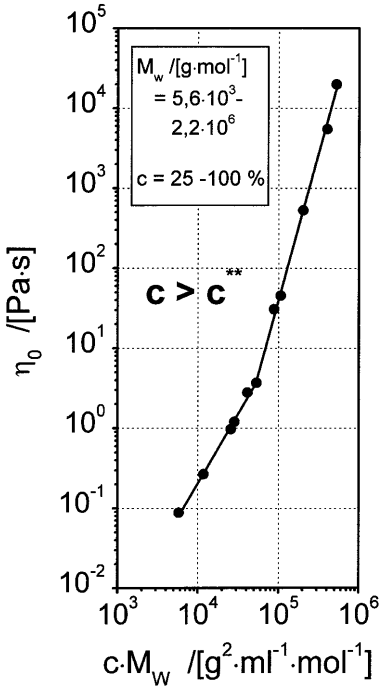

Fig. 1 Zero-shear viscosity η_0 vs $c \cdot M_w$ for concentrated solutions of polystyrene in *n*-butyl benzene. Data from Graessley (1974)

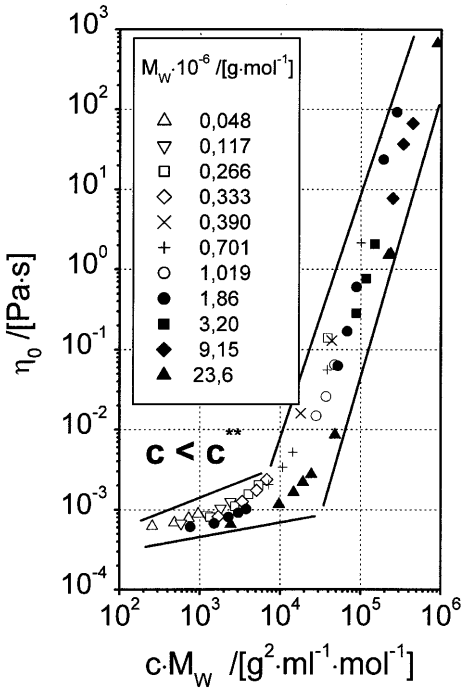

Fig. 2 Zero-shear viscosity η_0 vs $c \cdot M_w$ for moderately concentrated solutions of polystyrene in toluene. Data from Kulicke and Kniewske (1984)

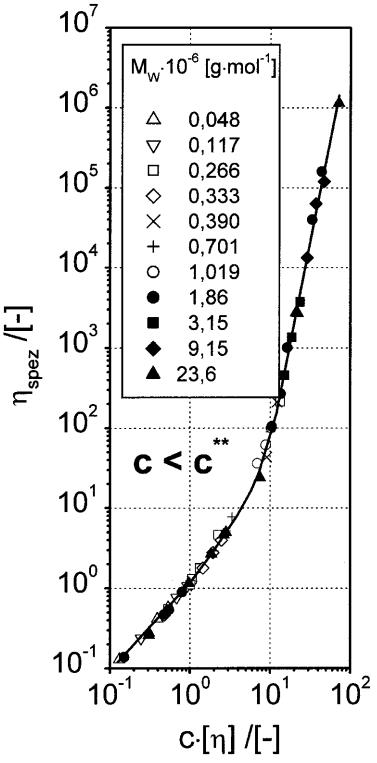

Fig. 3 Specific viscosity, η_{spec}, vs the overlap parameter, c·[η], for moderately concentrated solutions of polystyrene in toluene. Data from Kulicke and Kniewske (1984)

$$\eta_0[\mathrm{mPa \cdot s}] = 4.81 \cdot 10^{-3} \cdot c \cdot M_w^{0.736} + 1.658 \cdot 10^{-5} \cdot c^2 \cdot M_w^{1.472} + 5.579 \cdot 10^{-13} \cdot c^{4.55} \cdot M_w^{3.35} + 0.558 \quad (1)$$

Steady state shear flow measurements

The number of entanglements in the Newtonian flow region is constant and independent of the shear rate. This was shown with the aid of steady state shear flow measurements in the range of moderately concentrated solutions (Kehler and Kulicke 1986). In this procedure a shear rate is imposed suddenly upon the resting viscoelastic polymer solution and the behavior of the shear stress is determined over time. In the region of low deformation the elastic component of the solution obeys Hooke's Law. The zero-shear modulus, G_0^A, of the solution can be determined from the linear dependence of the shear stress, τ_{21}, upon the deformation, γ:

$$G_0^A = \lim_{\gamma \to 0} \frac{\partial \tau_{21}}{\partial \gamma}; \gamma = \dot{\gamma} \cdot t \quad (2)$$

On the basis of theory of rubber elasticity, the number of entanglements, v_e, can be calculated from the shear modulus, G^A (Schurz 1974):

$$G^A = \upsilon_e \cdot R \cdot T \quad (3)$$

Determination of the number of entanglements according to Eqs. (2) and (3) is also possible from a solution that has undergone stationary shear (Kehler and Kulicke 1986) if the linear region of the shear gradient is recorded after a higher shear rate has been imposed (Fig. 4). As can be seen in Figs. 5 and 7, the shear modulus for shear rates in the Newtonian flow range corresponds to the zero-shear modulus, and the number of entanglements remains constant here. In the transition from 1 s^{-1} to 20 s^{-1}, the stress can be seen to overshoot the stationary value, which indicates a change in the temporary network structure. This overshooting was only observed in transitions to shear rates that were in the non-Newtonian flow range. Determination of the shear modulus for a shear rate of 20 s^{-1} (Fig. 6) results in clear decrease in the number of entanglements.

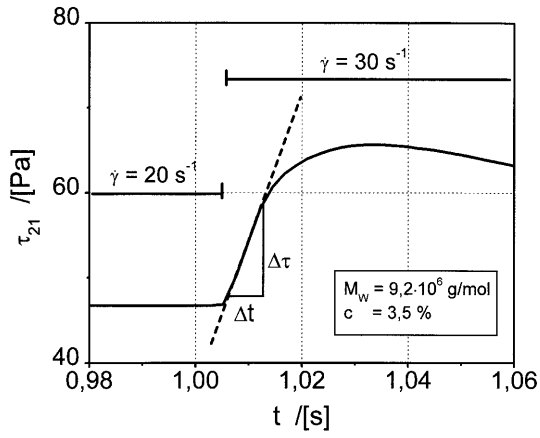

Fig. 4 Steady state shear measurement on polystyrene in toluene

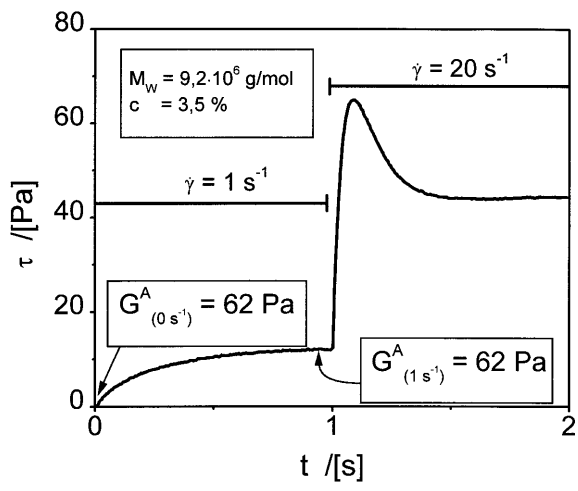

Fig. 5 Steady state shear measurement on polystyrene in toluene

Figure 7 provides a comparison of further entanglement densities for the flow curve determined from steady state shear measurements. In the non-Newtonian range the entanglement density decreases significantly, whereas it remains constant in the Newtonian region. This result supports the entanglement theory presented at the outset as being the cause for the shear-induced decrease in viscosity for moderately concentrated solutions. However, the entanglement figures determined are affected by the model as Eq. (3) is based on the underlying theory of a physical network, whereas the solutions considered only form temporary networks. If the viscosity is extrapolated to a completely disentangled state, it is found to lie several decades below the solvent viscosity. Nevertheless, using steady state shear measurements it was at least possible to detect qualitatively a reduction in the entanglement number within the non-Newtonian flow region.

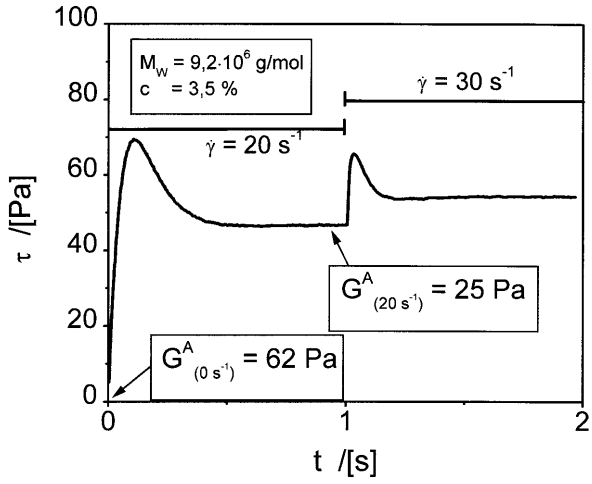

Fig. 6 Steady state shear measurement on polystyrene in toluene

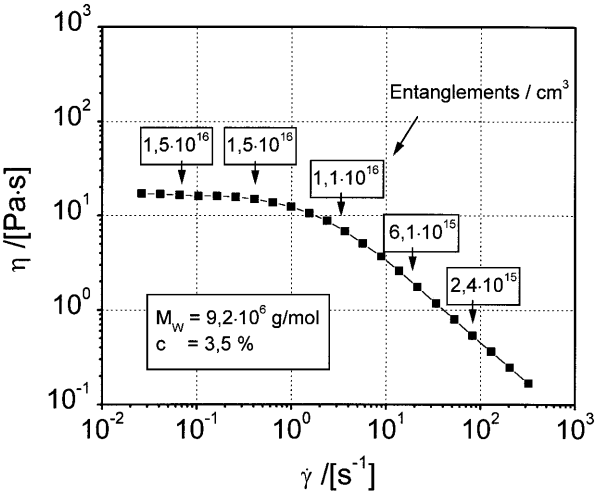

Fig. 7 Entanglement density from steady state shear measurements as a function of the shear rate. Polystyrene in toluene

Measurements of the flow birefringence and its orientation

To determine the influence of the deformation and orientation of the polymer coils on the viscosity of moderately concentrated network solutions, the alignment of the polymer segments was investigated in the shear field with the aid of rheo-optical measurements.

Polymer segments have different polarizabilities parallel and perpendicular to the main chain of the macromolecule. This gives rise to differing refractive indices along and perpendicular to the individual polymer segments (birefringence). Determination of the different refractive indices of a solution can therefore yield information on the mean orientation of the polymer segments and the proportion of oriented segments.

The flow birefringence, $\Delta n'$, determined in this case corresponds to the difference between the minimum and maximum refractive indices in the 1,2 plane of the shear field (Kalogianitis and van Egmond 1997). In the resting state the polymer segments are distributed isotropically; birefringence, and consequently an orientation of the refractive index tensor, is not present in this case. The formation of an anisotropic distribution of the segment orientation within a polymer coil is not induced until a shear field is imposed . The flow birefringence then represents a measure for the strength of the internal structural change, i.e., the deformation of a polymer coil. The birefringence as a function of the shear rate is shown for narrowly distributed polystyrene standards in toluene solution in Figs. 8a and 9a. The corresponding flow curves can be seen in Figs. 8b and 9b. Here, in each case, the overlap parameter of the solutions is above the critical value of $(c \cdot [\eta])^* = 8.2$, which describes the transition between a moderately concentrated particulate and a network solutions (Bouldin et al. 1988). Hence shape components of the birefringence, which occur in dilute solutions due to the difference between the refractive indices of isolated polymer coils and the solvent, can be excluded from these results. The birefringence measured is purely intrinsic and can only be attributed to alignment of the segments.

In Fig. 8a it can be seen, that, with a constant molar mass, M_w, the birefringence rises as the concentration, c, increases. This can also be seen in Fig. 9a for constant concentrations and increasing molar masses. These observations can be attributed to increasing intermolecular interactions, as the overlap parameter, $c \cdot [\eta]$, increases.

As can be seen from Figs. 8a, b and 9a, b, the birefringence rises linearly with the shear rate with a slope of one in the double logarithmic plot in the

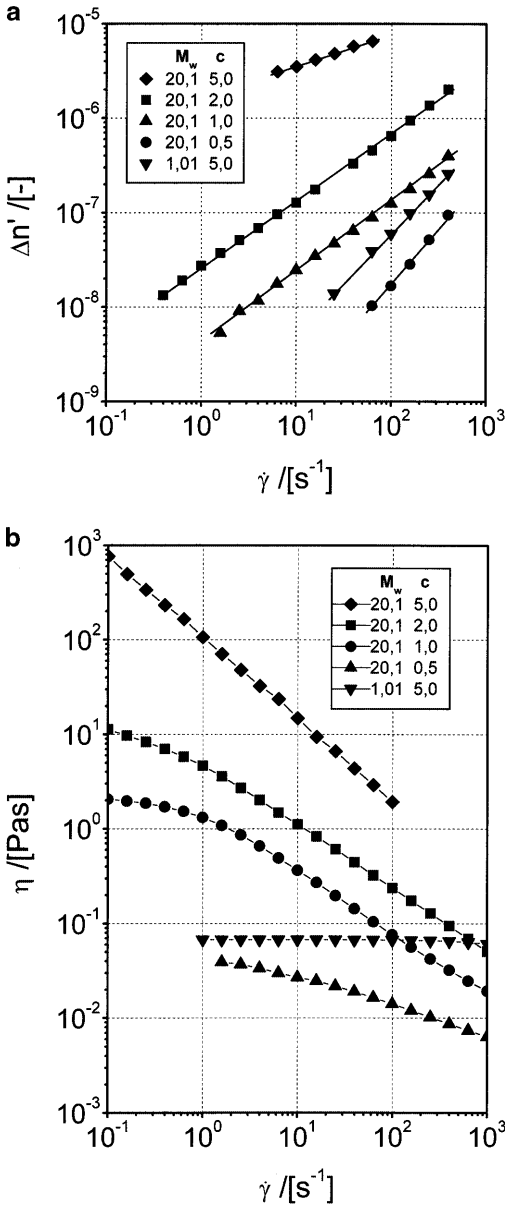

Fig. 8 **a** Flow birefringence, Δn′, against the shear rate of polystyrene in toluene. Molar mass, M_w, in 10^6 g/mol, concentration, c, in %. **b** Viscosity against the shear rate of polystyrene in toluene. Molar mass, M_w, in 10^6 g/mol, concentration, c, in %

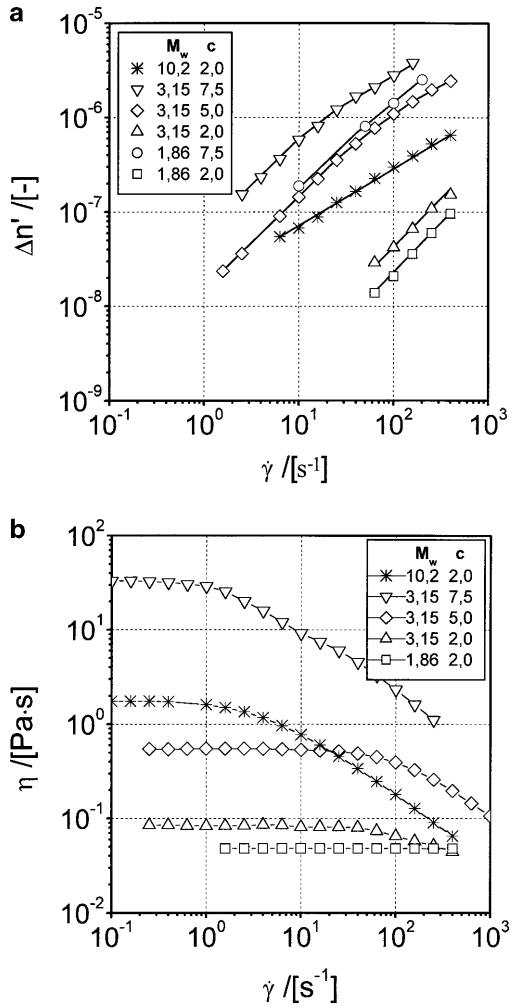

Fig. 9 **a** Flow birefringence, Δn′, against the shear rate of polystyrene in toluene. Molar mass, M_w, in 10^6 g/mol, concentration, c, in %. **b** Viscosity against the shear rate of polystyrene in toluene. Molar mass, M_w, in 10^6 g/mol, concentration, c, in %

Newtonian flow region. Hence a deformation of the polymer coils already occurs in this flow region, which has no influence on the viscosity. Samples measured in the non-Newtonian flow region (molar masses 20.1×10^6 g/mol (1%, 2%, and 5%) and 10.2×10^6 g/mol (2%)) show that the birefringence is also increasing linearly, but with a slope smaller than one. For the samples of molar mass 3.15×10^6 g/mol (5% and 7.5%) a transition from a slope of one to a lower gradient of the birefringence curve can clearly be seen. In this case the measurements of birefringence were carried out in the transition range of Newtonian to non-Newtonian flow.

The low gradient of the birefringence in the region of non-Newtonian flow indicates a smaller increase in the deformation of the polymer coils. This appears to contradict the theory according to which, due to inhibited relaxation capacity, pronounced deformation of the polymer coils and hence pronounced orientation in the direction of shear results in a decrease in viscosity. However, if one assumes from the start that pronounced stretching of the polymer coils results due to the entanglements in moderately concentrated network solutions, the smaller increase in the birefringence can then be explained by a decrease in the entanglement density. Indeed the polymer coils are stretched due to the fact that the longest relaxation time is larger than the

reciprocal shear rate in the non-Newtonian flow region. However, this effect is overcompensated by the coils being able to relax considerably better due to a decreasing entanglement density. Consequently, in the range of moderately concentrated network solutions, the influence of disentanglement on the lowering of the viscosity is considerably larger than the pronounced deformation and orientation of the coils.

In moderately concentrated and dilute particulate solutions there are no longer any entanglements. In these solution states, as the theory would expect, the pronounced deformation in the non-Newtonian flow-region is not reduced by a loss of entanglements and the slope of the birefringence curve can be larger than one. However birefringence measurements of polystyrene standards in the range of particle solutions cannot be carried out since the intensity of the measuring signal is outside of the measuring range of the apparatus employed.

The orientation angles, ϕ, of the birefringence correspond to the mean orientation of the polymer segments in the shear field, and hence to the orientation of the stretched polymer coils. Figures 10 and 11 show the orientation angles, ϕ, of the birefringence for the investigated polystyrene standards in toluene. Here an angle of 45° corresponds to a completely statistical orientation of the polymer coils, 0° to an orientation parallel to the direction of flow. The orientation shows the typical vertically mirrored S-curve, with a steep slope at high orientation angles and a less steep slope at low orientation angles.

In Fig. 10 it can clearly be seen that the orientation increases as the concentration rises, while shear rate and molar mass remain constant. This rising orientation can

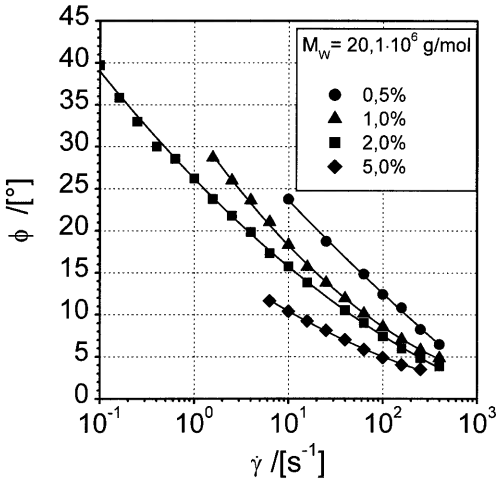

Fig. 10 Orientation angle, ϕ, of the birefringence as a function of the shear rate for polystyrene in toluene. Molar mass, M_w, in 10^6 g/mol, concentration, c, in %

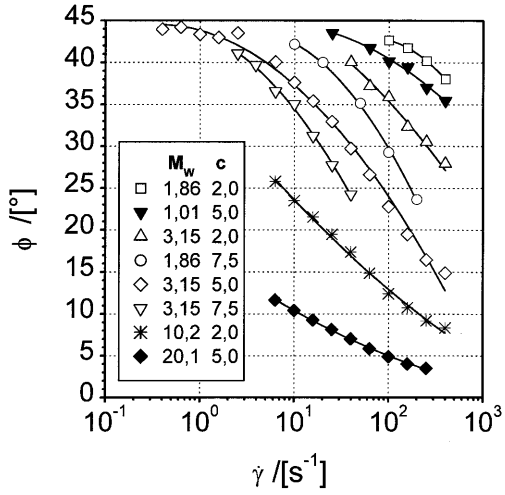

Fig. 11 Orientation angle, ϕ, of the birefringence as a function of the shear rate for polystyrene in toluene. Molar mass, M_w, in 10^6 g/mol, concentration, c, in %

be attributed to the increasing number of intermolecular interactions, particularly the increasing number of entanglements in a moderately concentrated network solution. Via the additional tensile forces on the entanglement points this leads to pronounced orientation of the polymer segments in the direction of flow.

Even at a constant concentration (Fig. 11), the orientation towards the direction of shear increases with constant shear rate and increasing molar mass. This can be attributed to the increasing overlap parameter $c \cdot [\eta]$, because the intrinsic viscosity rises with the molar mass. This leads to an increasing number of entanglements and therefore to increasing intermolecular interactions and a pronounced orientation of the polymer segments in the direction of flow.

Correlation of the flow birefringence and its orientation with the states of stress in moderately concentrated solutions

According to the stress-optical rule the birefringence and its orientation can be correlated with the principle stresses and their orientation in a sheared solution (Janeschitz-Kriegl 1983). The stress tensor, τ, of the solution is proportional to the refractive index tensor, n, with the stress-optical coefficient, C, as the proportionality factor. The flow birefringence, $\Delta n'$, in the 1,2 plain of the shear field is thus proportional to the first main stress difference, $\Delta\tau = \tau_I - \tau_{II}$, the orientation, ϕ, of the flow birefringence corresponds to the orientation, χ, of the first main stress difference. It is therefore possible to describe the birefringence and its orientation depending on critical parameters of the flow curve by replacing the principal stresses with known empirical models. This

presupposes that the stress-optical rule is fulfilled over the shear range considered. The validity of the stress-optical rule for the polystyrene solutions in toluene has been confirmed on numerous occasions (Janeschitz-Kriegl 1983; Otter 1967).

Flow birefringence depending on the states of stress

The following applies for the first main stress difference (Macosco 1994):

$$\Delta\tau = \sqrt{4 \cdot \tau_{21}^2 + N_1^2} \tag{4}$$

The shear stress, τ_{21}, can be accounted for via the modified CARREAU model (Yasuda et al. 1981; Gahleitner and Sobczak 1989):

$$\tau_{21} = \eta_0 \cdot \dot{\gamma} \cdot \left[1 + \left(\frac{\dot{\gamma}}{\dot{\gamma}_{crit}}\right)^b\right]^{\frac{n}{b}} \tag{5}$$

Here n corresponds to the flow curve gradient in the non-Newtonian range, b is a parameter that describes the width of the transition range between Newtonian and non-Newtonian flow. The first normal stress difference, N_1, can be described in a similar way to the modified Carreau model. A description via the mirror relation according to Gleißle (1982) is not suitable, because in the non-Newtonian shear range it yields the same gradient of $n+1$ for the first normal stress difference, N_1, as for the shear stress, τ_{21}.

The gradient of the first normal stress difference in the non-Newtonian flow region is assumed to be $2(n+1)$, i.e., twice the shear stress gradient, if the first normal stress difference is described in a similar way to the modified Carreau model:

$$N_1 = \Psi_{1,0} \cdot \dot{\gamma}^2 \cdot \left[1 + \left(\frac{\dot{\gamma}}{\dot{\gamma}_{crit}}\right)^b\right]^{\frac{2 \cdot n}{b}} \tag{6}$$

If $\Psi_{1,0}$ is substituted according to Eq. (7) (Macosco 1994):

$$\Psi_{1,0} = \frac{2 \cdot \eta_0}{\dot{\gamma}_{crit}} \tag{7}$$

the following dependence of birefringence upon shear rate is obtained according to Eqs. (4), (5) and (6):

$$\Delta n' = 2C \cdot \eta_0 \cdot \dot{\gamma} \cdot \sqrt{\left[1 + \left(\frac{\dot{\gamma}}{\dot{\gamma}_{crit}}\right)^b\right]^{\frac{2 \cdot n}{b}} + \left(\frac{\dot{\gamma}}{\dot{\gamma}_{crit}}\right)^2 \cdot \left[1 + \left(\frac{\dot{\gamma}}{\dot{\gamma}_{crit}}\right)^b\right]^{\frac{4 \cdot n}{b}}} \tag{8}$$

In order to calculate the birefringence over the entire flow range, the following parameters have to be known: zero shear viscosity, η_0, critical shear rate, $\dot{\gamma}_{crit}$, gradient of the flow curve in the non-Newtonian region, n, the overlap parameter, b, and the stress-optical coefficient, C. In Fig. 12 the birefringence values in accordance with Eq. (8) are compared with the experimental data for the investigated samples from Figs. 8a and 9a. For the samples which had experimentally inaccessible zero shear viscosity ranges η_0 was calculated according to the structure-property relationship in Eq (1). According to this, a good description of the birefringence is also possible with Eq. (8) in the non-Newtonian region.

For the Newtonian region ($\dot{\gamma} \ll \dot{\gamma}_{crit}$), Eq. (8) transforms to

$$\underset{\dot{\gamma} \ll \dot{\gamma}_{crit}}{\Delta n'} = 2 \cdot C \cdot \eta_0 \cdot \dot{\gamma} \tag{9}$$

Therefore in a double-logarithmic plot of $\Delta n'/\eta_0$ vs $\dot{\gamma}$ the Newtonian flow regions should lie on the straight line $2 \cdot C\ \dot{\gamma}$ with the slope of 1. In Fig. 13 this plot has been performed for the polystyrene standards from Figs. 8a and 9a. In addition the values $\Delta n'/\eta_0$ calculated from Eq. (8) have been plotted.

It can be clearly seen that the Newtonian regions of the various molar masses and concentrations coincide on the straight line $\Delta n'/\eta_0 = 2 \cdot C\ \dot{\gamma}$.

The straight line Eq. (9) agrees with the shear stress component of the stress-optical rule (Fuller 1995) (Eq. 10) if one assumes random orientation angles ($\phi = 45°$) and that the viscosity is equal to the zero-shear viscosity (Kulicke et al. 1999):

$$\tau_{21} = \frac{1}{2 \cdot C} \cdot \Delta n' \cdot \sin 2\phi \tag{10}$$

In the non-Newtonian region ($\dot{\gamma} \gg \dot{\gamma}_{crit}$, $n > -1$) Eq. (8) transforms to

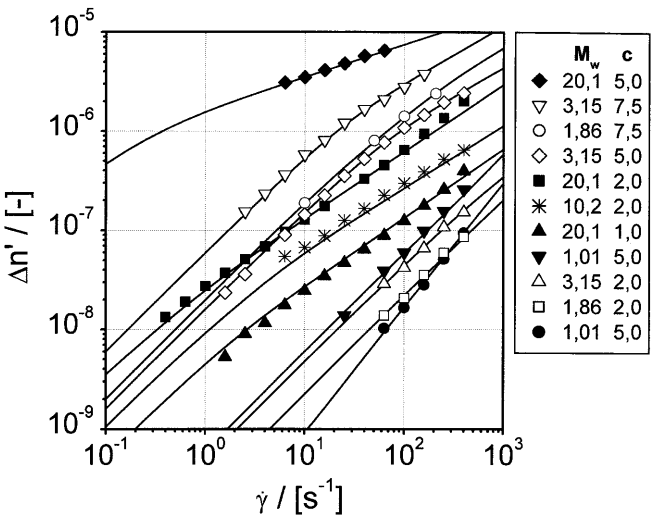

Fig. 12 Flow birefringence, $\Delta n'$, against the shear rate of polystyrene in toluene. Molar mass, M_w, in 10^6 g/mol, concentration, c, in %. The *continuous lines* represent the theoretical birefringence according to Eq. (8)

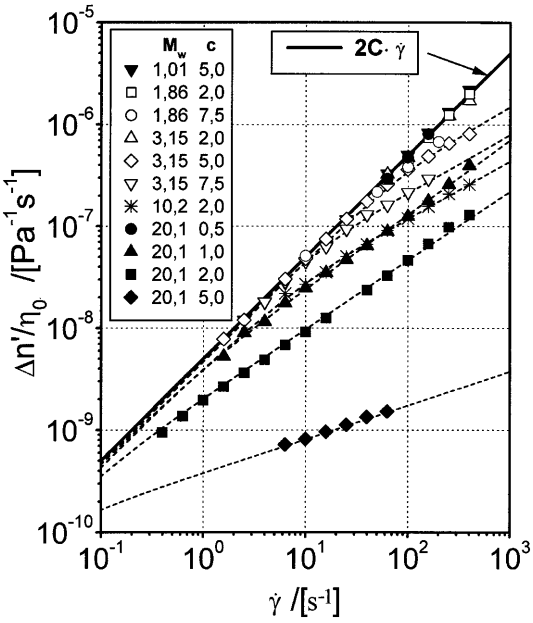

Fig. 13 Normalized flow birefringence, $\Delta n'/\eta_0$, against the shear rate of polystyrene in toluene. Molar mass, M_w, in 10^6 g/mol, concentration, c, in %. The *continuous line* corresponds to the theoretical birefringence, $\Delta n'/\eta_0$, of the Newtonian flow region. The *broken lines* represent the birefringence, $\Delta n'/\eta_0$, according to Eq. (8)

$$\underset{\dot{\gamma}\gg\dot{\gamma}_{crit}}{\Delta n'} = \frac{2\cdot C\cdot\eta_0}{\dot{\gamma}_{crit}^{(2\cdot n+1)}}\cdot\dot{\gamma}^{(2n+2)} \tag{11}$$

In the double-logarithmic plot the birefringence again has the shape of a straight line, the gradient of which is dependent upon the flow curve gradient, n, in the non-Newtonian region and which has the magnitude of $2n+2$. Hence for flow curve gradients between −0.5 and the boundary case −1, the gradient becomes smaller in the non-Newtonian flow region. As can be seen from Fig. 13, the normalized birefringence curves of the molar masses 20.1×10^6 g/mol (1%, 2%, and 5%) and 10.2×10^6 g/mol (2%) lie below the curve for Newtonian flow and can be described with Eq. (11). The transition to a lower gradient of the birefringence curves in the samples of molar mass 3.15×10^6 g/mol (5% and 7.5%) can be particularly clearly seen. The measurements of birefringence here were carried out in the transition range of Newtonian to non-Newtonian flow. In the lower shear rate range both curves lie on the straight lines complying with Eq. (9), whereas the gradient in the range of the critical shear rate, $\dot{\gamma}_{crit}$, decreases until the new limiting gradient according to Eq. (11) has been attained (Figs. 12 and 13).

For flow curve gradients between −0.5 and 0 the gradient of the birefringence curve according to Eq. (11) becomes greater than one (Fig. 14), hence the deformation in the non-Newtonian flow region increases more sharply. However, the measurement of a birefringence curve slope greater than 1 could not be carried out for the polystyrene standards. Investigations into the dependence of the flow curve gradient, n, on the overlap parameter, $c[\eta]$, have shown (Bouldin et al. 1988) that n only adopts values between 0.5 and 0 below an overlap parameter of 11.5 (Fig. 15).

With a critical overlap parameter of $(c\cdot[\eta])^* = 8.2$ these gradients then only occur in moderately concentrated and dilute particulate solutions (Bouldin et al. 1988). In these states of solution the intensity of the measuring signals lay outside of the measuring range of the apparatus employed.

Comparison of the orientation of the birefringence with the orientation of non interacting polymer coils

A theoretical orientation, ϕ, of the polymer coils in the shear field can be calculated from a distribution function for rotational ellipsoids first suggested by Peterlin (Peterlin and Stuart 1939):

$$F = \sum_{h=0}^{\infty}\sum_{k=0}^{h}\left[a_{hk}\left(\frac{\dot{\gamma}}{D_R},p\right)\cdot\cos(2\,k\cdot\phi) + b_{hk}\left(\frac{\dot{\gamma}}{D_R},p\right)\cdot\sin(2\,k\cdot\phi)\right]\cdot P_{2\,h}^{2\,k}(\cos\psi) \tag{12}$$

This distribution function takes into account the axial ratio, p, of the polymer coils and their rotary diffusion coefficient, D_R (Gans 1928), but does not include any intermolecular interactions. It thus enables the orientation of a polymer coil to be considered in different

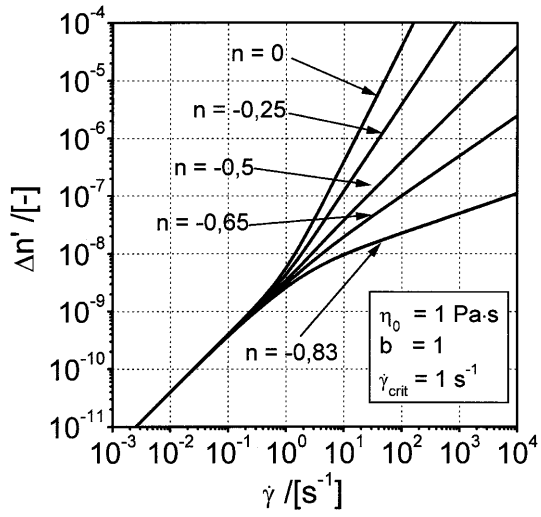

Fig. 14 Theoretical birefringence according to Eq. (8) for various flow curve gradients, n

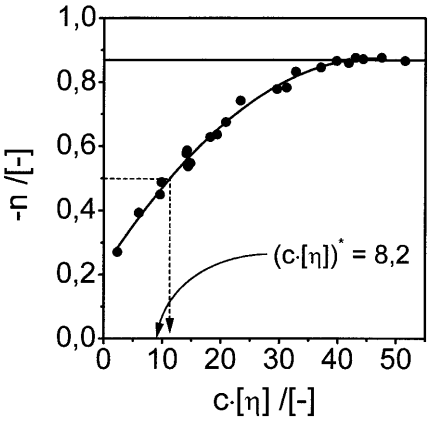

Fig. 15 Flow curve gradient, n, of the non-Newtonian region as a function of the overlap parameter, c·[η], for polystyrene in toluene. Data from Bouldin et al. (1988)

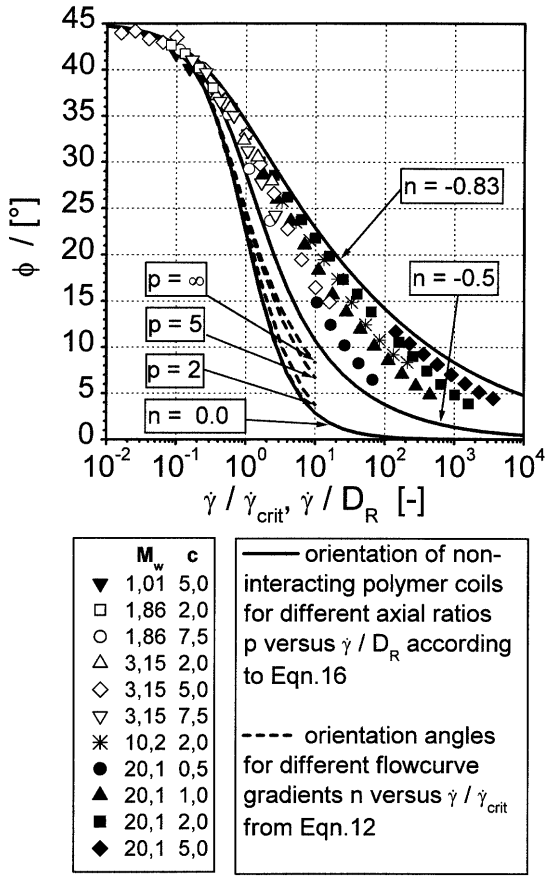

Fig. 16 Theoretical and experimental orientation angles, ϕ, of the birefringence against the normalized shear rates for polystyrene in toluene. Molar mass, M_w, in 10^6 g/mol, concentration, c, in %

deformation states without interactions with other molecules via entanglement points. The results of approximations for this distribution function according to Nakagaki and Heller (1975) for the orientation angles ϕ of different axial ratios, p (p = 1, 2, 5, ∞), are plotted in Fig. 16 as a function of a reduced shear rate, $\dot{\gamma}_{red} = \dot{\gamma}/D_R$.

In an analogous manner to the birefringence, a relationship to the shear rate can also be derived for the orientation of the birefringence from the stress states of the solution, if the stress-optical rule is valid. The following applies for the orientation angle, χ, of the first main stress, τ_I, to the direction of flow, which corresponds to the orientation angle, ϕ, of the birefringence (Macosco 1994):

$$\chi = \frac{1}{2}\arctan\left(2 \cdot \frac{\tau_{21}}{N_1}\right) \tag{13}$$

If the shear stress is substituted according to Eq. (5) and the first normal stress difference to Eq. (6) and (7), the following expression is obtained for the orientation angle, ϕ, of the birefringence:

$$\phi = \frac{1}{2}\arctan\left(\frac{\dot{\gamma}_{crit}}{\dot{\gamma}} \cdot \left[1 + \left(\frac{\dot{\gamma}}{\dot{\gamma}_{crit}}\right)^{b}\right]^{-\left(\frac{n}{b}\right)}\right) \tag{14}$$

Below $\dot{\gamma}_{crit}$, Eq. (14) becomes

$$\underset{\dot{\gamma} \ll \dot{\gamma}_{crit}}{\phi} = \frac{1}{2} \cdot \arctan\left(\frac{\dot{\gamma}_{crit}}{\dot{\gamma}}\right) \tag{15}$$

According to Eq. (15) the orientation angles ϕ should therefore coincide in the Newtonian region ($\dot{\gamma} \ll \dot{\gamma}_{crit}$,) if plotted against the reduced shear rate $\dot{\gamma}/\dot{\gamma}_{crit}$. In Fig. 16 this plot is shown for the experimentally determined orientation angles.

Accordingly, in the Newtonian flow range the orientation angle is only dependent upon the shear rate and the shape of the curves is the same for all concentrations and molar masses or solution states. The theoretical orientations in Fig. 16 from the distribution function (Eq. 12) also agree below the critical shear rate as well as orientation angles calculated in accordance with Eq. (14) for different flow curve gradients (n = 0, −0.5, −0.83). The axial ratio, p, and consequently the degree of deformation have no influence on the curve shape of the orientation in the Newtonian flow range.

For the non-Newtonian flow range, Eq. (14) becomes

$$\underset{\dot{\gamma} \gg \dot{\gamma}_{crit}}{\phi} = \frac{1}{2} \cdot \arctan\left(\frac{\dot{\gamma}_{crit}^{(n+1)}}{\dot{\gamma}^{(n+1)}}\right) \tag{16}$$

The orientation angle is then dependent upon the flow curve gradient, n, and therefore, according to Fig. 15, upon the overlap parameter. In Fig. 16 the experimental orientation angles of the non-Newtonian flow region lie between the calculated curves from Eq. (14) for flow curve gradients n = −0.5 and n = −0.82 and can be described with Eq. (14).

If a flow curve gradient of $n = 0$ is assumed above the limiting case, $\dot{\gamma}_{crit}$, Eq. (16) also matches Eq. (15) above $\dot{\gamma}_{crit}$. In this case the orientation angles also agree with the angles calculated from the distribution function (Eq. 12) for an undeformed coil (axial ratio, $p = 1$).

The influence of a deformation of the coils on the orientation angle can be seen clearly in Fig. 16. The experimentally determined orientation angles are significantly above the values calculated from the distribution function (Eq. 12) even for marked deformations ($p \rightarrow \infty$). In this case, too, the observed orientation angles are more likely to be accounted for by the intermolecular interactions (approximately 85%). A reduction in the entanglement density in the non-Newtonian flow range results in a reduction of the orientating tensile forces acting on the entanglement points. Therefore the experimental orientation angles are much higher than the orientation angles caused by a deformation of the polymer coils alone according to Eq. (12).

Conclusions

The flow behavior of the polymer standard system polystyrene in toluene was investigated for different molar masses and concentrations in the region of a moderately concentrated network solution.

With steady state shear flow measurements it could be shown that in the non-Newtonian flow range the entanglement density decreases significantly, whereas it remains constant in the Newtonian region.

Rheo-optical measurements showed that the birefringence as well as its orientation towards the direction of the shear flow rises with the concentration or the molar mass, due to increasing intermolecular interactions with a rising overlap parameter $c \cdot [\eta]$.

The flow birefringence and its orientation can be described over the whole range of the flow curve with new equations derived from the stress states of a sheared solution using the stress-optical rule. It could be shown, that outgoing from these equations in the Newtonian flow region a reduced birefringence $\Delta n'/\eta_0 = f(\dot{\gamma})$ and a reduced orientation $\phi = f(\dot{\gamma}/\dot{\gamma}_{crit})$ can be plotted, independent from concentration and molar mass.

For moderately concentrated solutions the birefringence increases linearly with the shear rate with a slope of one in the double logarithmic plot in the Newtonian flow region. In the non-Newtonian flow region the birefringence also increases linearly, but with a slope smaller than one. Furthermore in moderately concentrated network solutions the shape of the orientation curves in the non-Newtonian flow region shows a significantly smaller increase of the orientation than calculated curves for polymer coils deformed in the flow field without intermolecular interactions. These observations, the loss of orientation, and the small birefringence gradients, can be attributed to a decreasing entanglement density in the non-Newtonian flow region and lead to the assumption that in this state of solution the loss of viscosity is mainly caused by the disentanglements and not by an increased deformation of the polymer coil and a greater degree of orientation in the shear field.

References

Baumgärtel M, Willenbacher M (1996) The relaxation of concentrated polymer solutions. Rheol Acta 35:168–185

Bird RB, Armstrong RC, Hassanger O (1977) Dynamics of polymeric liquids. Wiley, New York

Bouldin M, Kulicke W-M, Kehler H (1988) Prediction of the non-Newtonian viscosity and shear stability of polymer solutions. Colloid Polym Sci 266:793–805

Bueche F (1952) Viscosity, self-diffusion, and allied effects in solid polymers. J Chem Phys 20:1959–1964

De Gennes PG (1971) Reptation of a polymer chain in the presence of fixed obstacles. J Chem Phys 55:572–579

De Gennes PG (1979) Scaling concepts in polymer physics. Cornell University Press, Ithaca, New York

De Gennes PG, Leger L (1982) Dynamics of entangled polymer chains. Ann Rev Phys Chem 33:49–61

Doi M (1983) Explanation for the 3,4-power law for viscosity of polymeric liquids on the basis of the tube model. J Polym Sci Polym Phys Ed 21:667–684

Doi M, Edwards SF (1978) Dynamics of concentrated polymeric systems. J Chem Soc Farad Trans 74:1802–1818

Doi M, Edwards SF (1986) The theory of polymer dynamics. Oxford University Press, Oxford

Elias H-G (1996) Polymere, von Monomeren zu Makromolekülen und Werkstoffen. Hüthig & Wepf Verlag, Zug

Fixman M (1966) Polymerdynamics:nonnewtonian intrinsic viscosity. J Chem Phys 45:793–803

Flory PJ (1975) Die Konformation linearer Makromoleküle. Angew Chem 87:787–822

Fuller GG (1995) Optical rheometry of complex fluids. Oxford University Press, New York

Gahleitner M, Sobczak M (1989) Bedeutung der Nullviskositätsbestimmung für das Modelieren von Fließkurven. Kunststoffe 79:1213–1216

Gans R (1928) Zur Theorie der Brownschen Molekularbewegung. Ann Phys 86:628–656

Gleißle W (1982) Rheol Acta 16:484

Graessley WW (1965) Molecular entanglement theory of flow behavior in amorphous polymers. J Chem Phys 43:2696–2703

Graessley WW (1967) Viscosity of entangling polydisperse polymers. J Chem Phys 47:1942–1953

Graessley WW (1974) The entanglement concept in polymer rheology. Adv Polym Sci 16:1–179

Graessley WW, Hazelton R, Lindeman R (1967) The shear-rate dependence of viscosity in concentrated solutions of narrow distributed polystyrene. Trans Soc Rheol 11:267–285

Grigorescu G, Kulicke W-M (2000) Prediction of viscoelastic properties and shear stability of polymers in solution. Adv Polym Sci 152:1–45

Janeschitz-Kriegl H (1983) Polymer melt rheology and flow birefringence. Springer, Berlin Heidelberg New York
Johnson SJ, Frattini GG, Fuller GG (1985) Simultaneous dichroism and birefringence measurements of dilute colloidal suspensions in transient shear flow. J Colloid Interface Sci 104:440–455
Kalogianitis SG, van Egmond JW (1997) Full tensor rheometry of polymer fluids. J Rheol 41:343–364
Kehler H, Kulicke W-M (1986) Bestimmung der Verhängunszahlen in ruhenden und strömenden Polymer-Lösungen. Chem Ing Tech 58:802–804
Kniewske R, Kulicke W-M (1983) Study on the molecular weight dependence of dilute solution properties of narrowly distributed polystyrene in toluene and in the unperturbed state. Makromol Chem 184:2173–2186
Kulicke W-M, Arendt O (1997) Rheo-optical investigation of biopolymer solutions and gels. Applied Rheology 7:12–18
Kulicke W-M, Kniewske R (1984) The shear viscosity dependence on concentration, molecular weight and shear rate of polystyrene solutions. Rheol Acta 23:75–83
Kulicke W-M, Reinhardt U, Fuller GG, Arendt O (1999) Characterization of the flow properties of sodium carboxymethylcellulose via mechanical and optical techniques. Rheol Acta 38:26–33
Macosco CW (1994) Rheology – principles, measurements and applications. VCH Publishers, New York
Nakagaki M, Heller W (1975) Recomputation of certain functions in the Peterlin-Stuart theory of flow birefringence and directions for the evaluation of experimental data in terms of molecular weight and molecular dimensions. J Chem Phys 62:333–340
Otter D (1967) Dynamic properties of some polymeric systems. Dissertation, Univ Leiden
Pahl M, Gleißle W, Laun H-M (1995) Praktische Rheologie der Kunstoffe und Elastomere. VDI-Verlag, Düsseldorf
Peterlin A (1960) Gradient dependence of the intrinsic viscosity of freely flexible linear macromolecules. J Chem Phys 33:1799–1802
Peterlin A (1961) Einfluß der endlichen Moleküllänge auf die Gradientenabhängigkeit ds Staudingerindex. Makromol Chem 44–46:338–346
Peterlin A, Stuart HA (1939) Z Phys 112:1
Reinhardt UT, Meyer de Groot EL, Fuller GG, KulickeW-M (1995) Rheo-optical characterisation of the tobacco mosaic virus. Macromol Chem Phys 196:63–74
Schurz J (1974) Struktur-Rheologie. Berliner Union GmbH, Stuttgart
Yasuda K, Armstrong RC, Cohen RE (1981) Rheol Acta 20:163